

Impact of band structure on wave function dissipation in field emission resonanceWei-Bin Su ^{1,*}, Shin-Ming Lu ¹, Ho-Hsiang Chang,¹ Horng-Tay Jeng ^{2,1,3,†}, Wen-Yuan Chan ¹,
Pei-Cheng Jiang ¹, Kung-Hsuan Lin ¹ and Chia-Seng Chang¹¹*Institute of Physics, Academia Sinica, Nankang, Taipei 11529, Taiwan*²*Department of Physics, National Tsing Hua University, Hsinchu 30013, Taiwan*³*Physics Division, National Center for Theoretical Sciences, Hsinchu 30013, Taiwan* (Received 8 January 2021; revised 20 February 2022; accepted 22 April 2022; published 6 May 2022)

We demonstrated on Ag(111) and Ag(100) surfaces that the reciprocal of the field emission resonance (FER) linewidth, which is proportional to the mean lifetime of resonant electrons in FER, may vary with the electric field. The variation on Ag(111) was nearly smooth, whereas that on Ag(100) was sporadic and fluctuated remarkably. This drastic difference can be explained through their dissimilar projected bulk band structures and the ensemble interpretation of quantum mechanics, according to which all resonant electrons are governed by a single wave function (WF). Ag(100) has an energy gap above its vacuum level, whereas Ag(111) does not. Consequently, the dissipation rate of the WF, which is relevant to the FER linewidth, on Ag(111) was almost stable, whereas that on Ag(100) fluctuated. The fluctuation originated from the quantum trapping effect and surface dipole layer (SDL) on Ag(100) surface. Through FER linewidth, we also demonstrated that SDLs of Cu(100) and Ag(100) are different.

DOI: [10.1103/PhysRevB.105.195411](https://doi.org/10.1103/PhysRevB.105.195411)**I. INTRODUCTION**

Field emission resonance (FER) [1] in scanning tunneling microscopy (STM) [2,3] is a versatile technique for investigating various physical phenomena and properties, such as the atomic structure of an insulator [4], plasmon-assisted electron tunneling [5], resistance at the nanometer scale [6], light emission [7–9], the dynamics [10,11] and lateral quantization [12–14] of surface electrons above the vacuum level, the work functions of thin films [15–22], surface reconstructions [23–25], sharpness [8,26,27] and field enhancement factors [28] of STM tips, and bandgaps [25]. Recently, we demonstrated on bulk MoS₂ that FER can be used to observe the quantum trapping that leads to the variation in the FER linewidth being as high as one order of magnitude [29]. This case on the MoS₂ implies that the lifetime of FER electrons can be sensitive to the physical properties of the surface.

In quantum mechanics, the *wave function* (WF) describes the wave behavior of particles. In FER, the WF is a standing wave. Previous studies have demonstrated that resonant electrons can exit FER through surface transmission [25] or light emission [7,8], which implies that the WF is not stationary but can be dissipated. WF dissipation (WFD) in FER and the correlation of WFD with surface properties have been seldom investigated. In this paper, we demonstrated on Ag(111) and Ag(100) surfaces that WFD can be studied by using the FER linewidth and electric field of FER formation. Ag(100) and Ag(111) were selected for comparison because, in their projected bulk band structures, Ag(100) has an energy gap

above its vacuum level, but Ag(111) does not [30]. The results indicated that the dissipation rate of the WF in first-order FER on Ag(111) was higher than that on Ag(100). Furthermore, the dissipation rate on Ag(111) was nearly constant, but that on Ag(100) fluctuated remarkably. To explain these results, we adopted the ensemble interpretation of quantum mechanics [31], according to which all resonant electrons in FER are governed by a single WF. In fact, many interpretations have been proposed [32]. In other words, FER may be a touchstone for verifying various interpretations, like the interference pattern in the double-slit experiment [33].

II. METHODS

In the experiment, clean Ag(111), Ag(100), and Cu(100) surfaces were prepared using ion sputtering followed by annealing at 600 °C for several cycles, then transferred to ultrahigh-vacuum STM operated at 78 or 5.5 K. FERs were observed through Z-V spectroscopy by using PtIr tips. The Z-V spectrum was differentiated using a numerical method to reveal FERs.

The surface electronic structures of Au(111) were calculated using the projector augmented wave approach [34], as implemented in the Vienna *Ab initio* Simulation Package [35] based on density functional theory (DFT). The local density approximation was used for the exchange-correlation functional. The spin-orbit coupling was considered in the self-consistent field (SCF) calculations with the cutoff energy of 230 eV for the plane-wave basis. Here, $12 \times 12 \times 1$ Γ -centered Monkhorst-Pack k-mesh over the two-dimensional (2D) Brillouin zone was used for the 60-layer Au slab calculations with the surface Au located at face-centered cubic (fcc), hexagonal close-packed (hcp), and ridge sites

*wbsu@phys.sinica.edu.tw

†jeng@phys.nthu.edu.tw

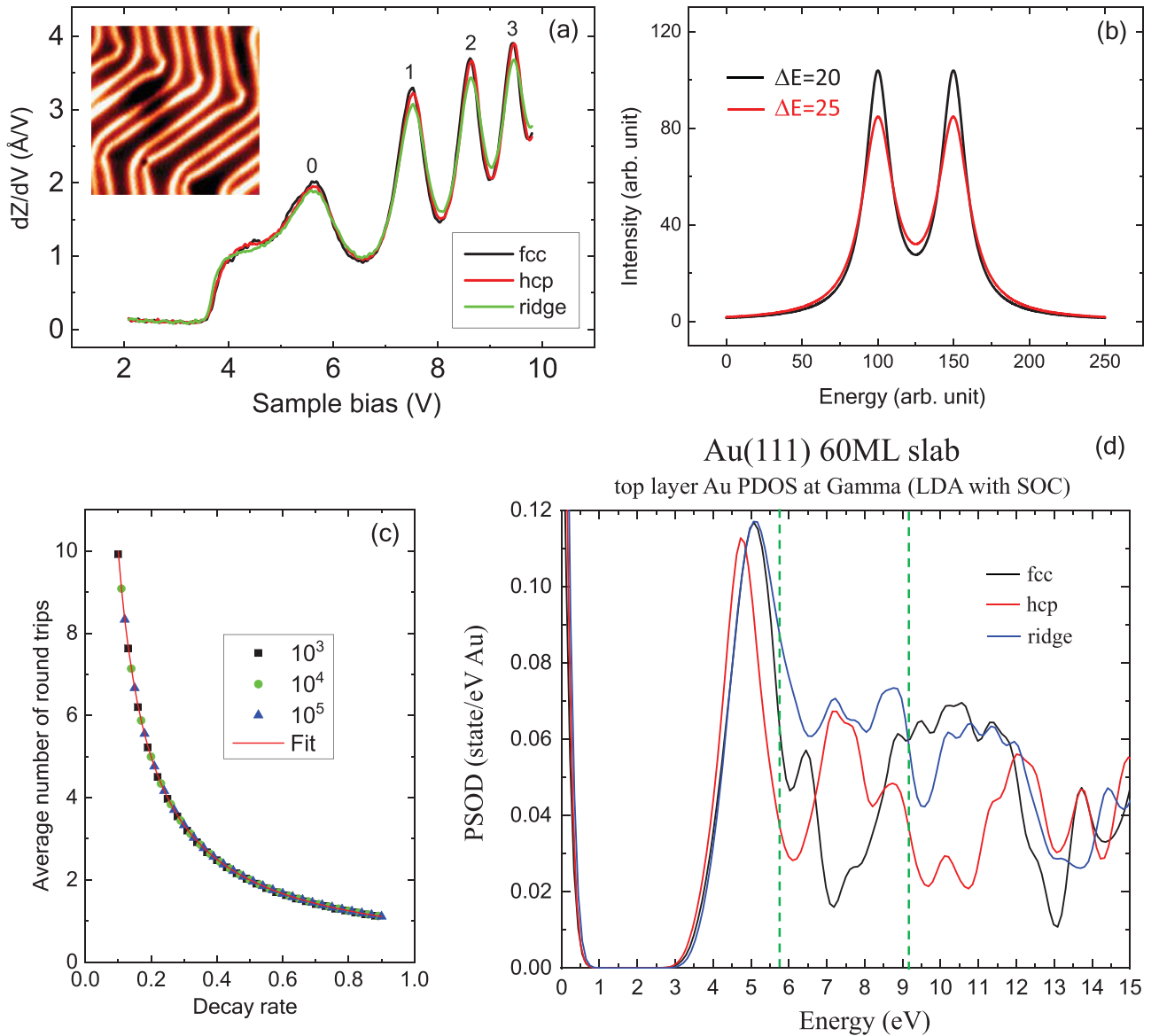


FIG. 1. (a) The field emission resonance (FER) spectra of the face-centered cubic (fcc), hexagonal close-packed (hcp), and ridge regions and topographical image of a reconstructed Au(111) surface (inset), drawn from Ref. [25]. (b) The valley intensity between two Lorentzian peaks with $\Delta E = 25$ is higher than that with $\Delta E = 20$ for a peak separation $E = 50$. By contrast, the peak intensities for $\Delta E = 25$ are lower. (c) $\langle j \rangle$ vs D for $N = 10^3$, 10^4 , and 10^5 , showing a trend that can be fit by a curve representing $\langle j \rangle = 1/D$. (d) Calculations of the partial density of states (PDOS) of the fcc, hcp, and ridge regions on Au(111) surface, based on the atomic model in Ref. [36].

separately, based on the atomic model in Ref. [36]. The vacuum thickness of 15 \AA well separating the slabs was adopted in all calculations. The energy convergence threshold was 10^{-4} eV in the SCF calculations, while the energy convergence threshold was 10^{-3} eV for the structure optimizations. The partial density of states (PDOS) was calculated at the Γ point of the 2D Brillouin zone to simulate the zone-center sensitive measurements.

III. RESULTS AND DISCUSSION

Our previous study [25] demonstrated that FER peaks observed on the reconstructed Au(111) surface [36] exhibit spatial variation [Fig. 1(a)]. The peak intensity at the ridge region was lower than that at the fcc and hcp regions, but

the opposite trend was observed for the intensity of the valley between FER peaks. This intensity difference was attributed to the higher electron transmissivity of the ridge region. In fact, this intensity variation also indicated that the linewidth ΔE of FERs at the ridge region was greater than that at the fcc and hcp regions. Figure 1(b) shows FER peaks simulated using the Lorentzian function under the same intensity integration and that, for a greater ΔE , the peak intensity is lower, but the intensity at the valley is higher, consistent with the experimental observation on Au(111). Therefore, ΔE may increase with an increase in transmissivity.

In the ensemble interpretation of quantum mechanics [31], all FER electrons are considered an ensemble governed by a single WF. When the electron transmissivity of the surface is between 0 and 1, because of partial transmission, WFD

occurs when the electrons impinge on the surface. Moreover, studies have demonstrated that light can be detected when observing FER [7,8], which implies that the light emission is also a pathway for WFD. A resonant electron eventually leaves FER through transmission or light emission. However, before leaving, the electron moves back and forth in round trips in the STM junction and forms the standing wave. WFD leads to decay of the probability $P(j)$ that resonant electrons remain in FER, where j is the number of round trips. Here, $P(j)$ can be defined as follows:

$$P(j) = (1 - D)^j, \quad (1)$$

where D is the decay rate of the probability per round trip, which is the sum of Γ_t (transmissivity) and Γ_l (decay rate due to light emission). Equation (1) suggests that the probability that a resonant electron stays in FER for $(j - 1)$ round trips but leaves FER in the j th round trip is $P(j - 1) - P(j)$. The average number of round trips $\langle j \rangle$ of all resonant electrons is as follows:

$$\langle j \rangle = \sum_{j=1}^{j=j_{\max}} j[P(j - 1) - P(j)], \quad (2)$$

where j_{\max} is the maximum number of round trips for which a resonant electron can remain in FER, depending on the number N of all resonant electrons in FER. Figure 1(c) presents a plot of $\langle j \rangle$ vs D , which was obtained using Eqs. (1) and (2) for $N = 10^3$, 10^4 , and 10^5 . The plots show a trend that $\langle j \rangle$ decreases with increasing D and is independent of N . This trend can be well fit by a curve representing $\langle j \rangle = 1/D$. Because N is $\sim 10^{10}$ for FER, the $\langle j \rangle$ vs D plot in the FER case should follow this curve. Since the ridge region on Au(111) has a higher Γ_t , $\langle j \rangle$ is smaller. A larger $\langle j \rangle$ indicates a longer mean lifetime. Thus, $\langle j \rangle$ is linearly proportional to $1/\Delta E$. Therefore, a higher Γ_t corresponds to a greater ΔE , which explains the wider FER on the ridge region. Moreover, it was suggested that a higher Γ_t is attributed to a larger density of states (DOS) above the vacuum level [25], which is verified by the DFT calculations, as shown in Fig. 1(d) (see Supplemental Material [37]). The PDOS at the ridge region in an energy range where FERs were observed (marked by dashed lines) is larger than those at the fcc and hcp regions.

Transmissivity is proportional to the DOS. Therefore, it can be suggested that Γ_t is zero for the electron energy in the energy gap. Because light emission is the only channel for WFD, the FER ΔE on a material with an energy gap should be different from that of a material without an energy gap. To verify this, Ag(100) and Ag(111) surfaces were selected because Ag(100) has an energy gap above its vacuum level, whereas Ag(111) does not, as depicted in Fig. 2. Figures 3(a) and 3(b) display typical FER spectra for Ag(111) and Ag(100), respectively, at 78 K under 10 pA. The numbers in the figure denote the order of the FERs. The horizontal dashed line in Fig. 3(b) indicates zero spectral intensity. The intensity of the valleys (marked by upward arrows) around the FER 1 peak are zero. The zero valley intensity reflects no DOS in the energy gap whose range is marked by vertical dashed lines according to the band structure of Ag(100) in Fig. 2. Therefore, the energy of FER 1 is in the energy gap. Because of zero DOS, resonant electrons of FER 1 cannot penetrate the surface. The

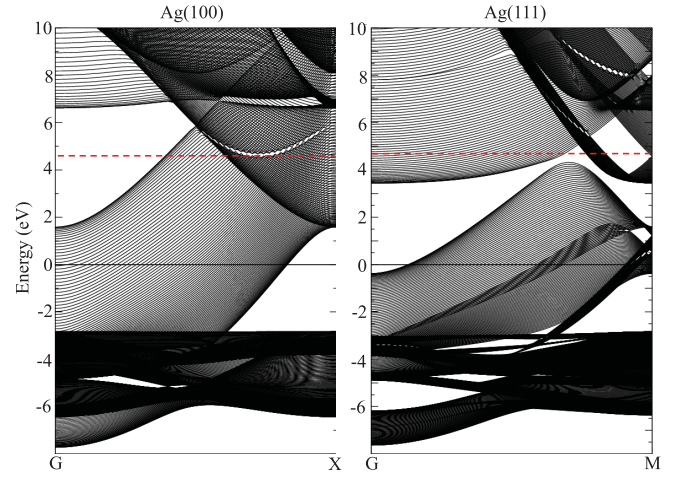


FIG. 2. Projected bulk band structures for Ag(100) (left) and Ag(111) (right) surfaces. Dashed lines indicate their vacuum levels. Ag(100) has an energy gap above its vacuum level, whereas Ag(111) does not.

zero valley intensity vanishes in Fig. 3(a) due to no energy gap.

Nevertheless, we noticed that the valley intensity at the left-hand side of the FER 0 peak is not zero (marked by a downward arrow), even though the energy of FER 0 is in the energy gap. FER 0 results from a quantized state formed in a potential dominated by the image potential because its energy is near the vacuum level. This nonzero valley intensity reflects that the resonant electrons in FER 0 have DOS available. Therefore, light emission is not the only decay channel for resonant electrons of FER 0. Previous studies of image-potential states have demonstrated that the electrons of image-potential states have a decay channel to bulk electrons [38,39]. Therefore, this nonzero valley intensity in the energy gap originates from the WF overlap between FER 0 and the bulk states. The overlap is negligible for FER 1, and thus, the valley intensity is zero. Figure 3(b) demonstrates that using tunneling spectroscopy to resolve the bandgap depends on the energy of tunneling electrons.

The potential of FERs of order >0 is the external potential typically approximated by a linear potential. Therefore, the energies of FERs are described as follows [40]:

$$E_n = E_{\text{vac}} + \alpha F_{\text{FER}}^{2/3} \left(n - \frac{1}{4}\right)^{2/3}, \quad (3)$$

where E_{vac} is the vacuum level, F_{FER} is the electric field of FER formation, $n = 1, 2, 3 \dots$ is the quantum number equal to the order number, and $\alpha = \left(\frac{\hbar^2}{2m}\right)^{1/3} \left(\frac{3\pi e}{2}\right)^{2/3}$. Figure 3(c) displays plots of the energies of the higher-order FERs in Figs. 3(a) and 3(b) vs $(n - \frac{1}{4})^{2/3}$. The results reveal that the data points of two cases can be fit favorably by lines for orders from 1 to 3, but for those beyond order 3, the data points deviate obviously from the linear fit. This deviation is attributed to the apex curvature of the tip, which enables the formation of FERs (order > 3) under a weaker field [27]. The lines in Fig. 3(c) are parallel, indicating that the F_{FER} of forming FERs 1–3 is equal for both spectra. This F_{FER} can also

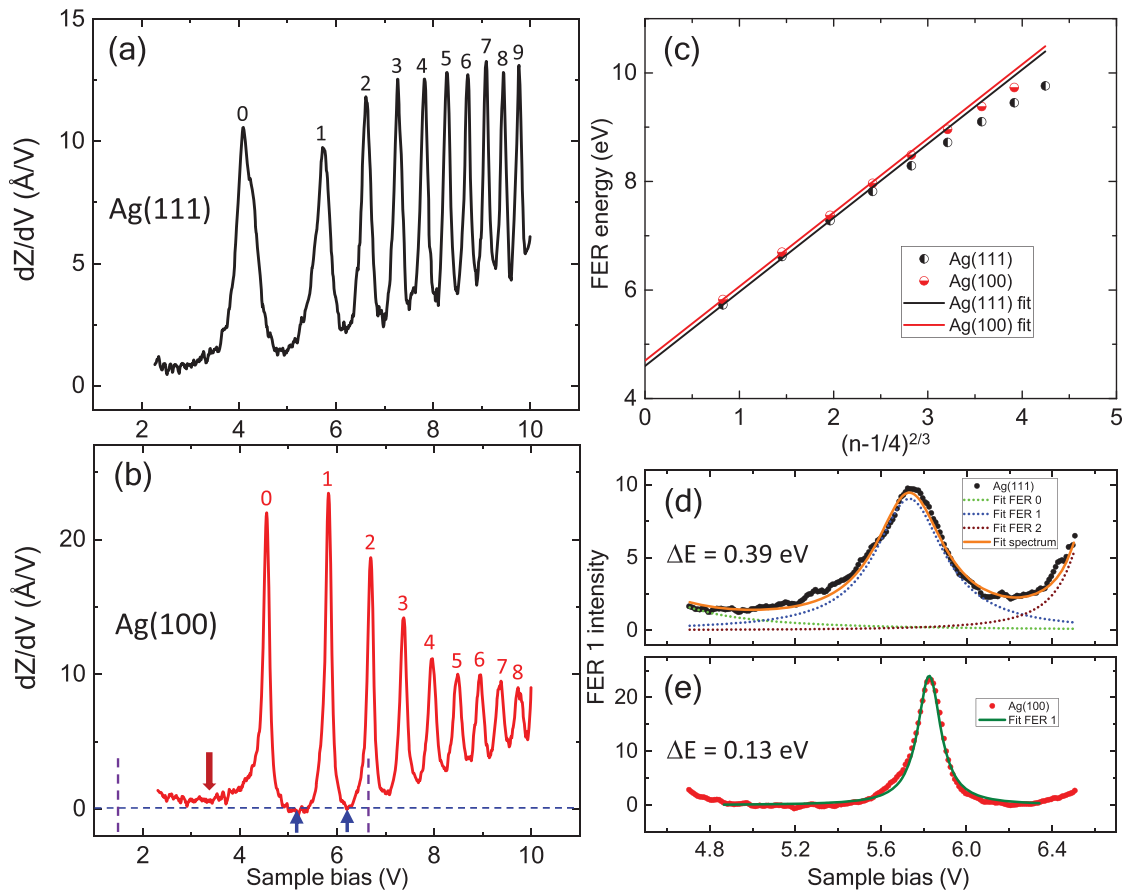


FIG. 3. Typical field emission resonance (FER) spectra acquired on (a) Ag(111) and (b) Ag(100). The horizontal dashed line in (b) indicates zero spectral intensity. The intensities of the valleys (marked by upward arrows) around the FER 1 peak are exactly zero, implying that Ag(100) has an energy gap and that FER 1 energy is in this energy gap, whose range is marked by vertical dashed lines according to the band structure of Ag(100) in Fig. 2. However, the valley intensity at the left-hand side of FER 0 peak is not zero (marked by a downward arrow). (c) Peak energies of the higher-order FERs in (a) and (b) vs $(n-\frac{1}{4})^{2/3}$. (d) FER 1 in (a), the ΔE of which is obtained from Lorentzian fitting and decomposition of the intensity superposition with FER 0 and FER 2. (e) FER 1 in (b), ΔE of which is simply obtained from Lorentzian fitting because of zero valley intensity.

be obtained from the slope of the line. Moreover, FER electrons are confined within a distance $s = (E_n - E_{\text{vac}})/eF_{\text{FER}}$ between the surface and the turning point. Consequently, the round-trip time t for resonant electron can be calculated using $2s = eF_{\text{FER}}t^2/m$. By combining this equation with Eq. (3), we obtain $t = \beta \frac{(n-\frac{1}{4})^{1/3}}{F_{\text{FER}}^{2/3}}$, where $\beta = (\frac{3m\hbar\pi}{e^2})^{1/3}$. The mean lifetime can be defined as $\langle j \rangle t$.

Because the energy of FER 1 is in the energy gap of Ag(100), here, we focus on the comparison of FER 1 on Ag(111) and Ag(100). Figures 3(d) and 3(e) display the FER 1 in Figs. 3(a) and 3(b), respectively. Although acquired under the same F_{FER} , the FER 1 on Ag(111) was considerably broader than that on Ag(100), as indicated by their ΔE , which was obtained from Lorentzian fittings. Here, F_{FER} can be tuned by adjusting the sharpness of the STM tip through the spontaneous change due to the thermal effect [29] (see Supplemental Material [37]) or by applying a voltage pulse. Therefore, ΔE under various F_{FER} can be investigated through FER spectra of various sharpness levels. Figure 4(a) displays $1/\Delta E$ vs F_{FER} plot, showing that the values on Ag(111) are prominently lower than those on Ag(100) within an F_{FER}

range. Moreover, the fluctuation of $1/\Delta E$ on Ag(100) is considerably greater than that on Ag(111). Figure 4(b) displays the $1/\Delta E$ vs F_{FER} plot for Ag(111) solely, which reveals that, on average, the data points follow a curve representing $1/\Delta E$, which is proportional to $F_{\text{FER}}^{-2/3}$. This proportionality can be confirmed by tuning the current to adjust F_{FER} at 5.5 K (see Supplemental Material [37]). Thus, the slight fluctuation in Fig. 4(b) can be attributed to various tip structures (discussed later). Because t is also proportional to $F_{\text{FER}}^{-2/3}$, $\langle j \rangle$ on Ag(111) is insensitive to F_{FER} and can be represented by $F_{\text{FER}}^{2/3}/\Delta E$. Therefore, D on Ag(111) is constant if the tip-structure effect is ignored, which is in agreement with Γ_t and Γ_l being independent of F_{FER} .

The round-trip time is a constant for a fixed potential, such as the image potential. Thus, for the image-potential states observed by two-photon photoemission [30,39], the contribution of the round-trip time to the lifetime of this quantum state is invisible. For the FER state, the potential is varied with the sharpness of the STM tip, leading to various round-trip times. The round-trip time playing a role in the lifetime of the quantum state becomes visible, as shown in Fig. 4(b). In

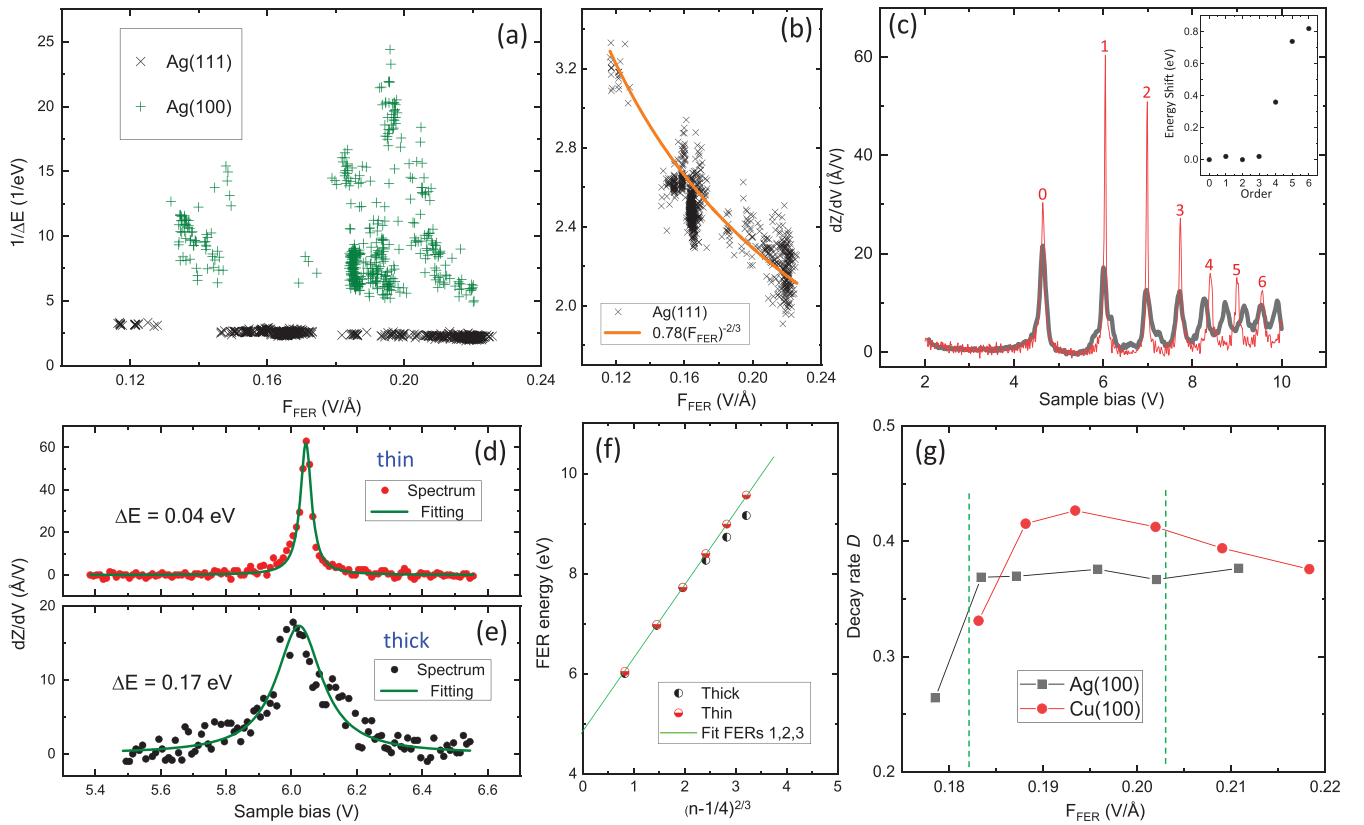


FIG. 4. (a) Plots of $1/\Delta E$ vs F_{FER} on Ag(111) and Ag(100). (b) $1/\Delta E$ vs F_{FER} on Ag(111) in (a), revealing that, on average, data points follow a curve representing $1/\Delta E$ proportional to $F_{\text{FER}}^{-2/3}$. (c) Two (thin and thick) spectra on Ag(100). Inset: energy shift between field emission resonances (FERs) of the same order vs order. (d) FER 1 in thin spectrum and extracted ΔE of 0.04 eV from fitting. (e) FER 1 in thick spectrum and extracted ΔE of 0.17 eV from fitting. (f): FER energy vs $(n-\frac{1}{4})^{2/3}$ plots of both spectra. The line is a fitting for data points of FERs 1, 2, and 3. (g) Decay rate D vs F_{FER} for Ag(100) and Cu(100). This kind of measurement was difficult to execute repeatedly because the scanning tunneling microscopy (STM) tip structure was liable to change when the tip was moved from one surface to the other via the coarse motion. Therefore, this figure has no error bar.

addition, Fig. 4(b) implies that the particle nature of electrons can be revealed in the FER state because the round-trip time is derived from the classical mechanics. Using the data in Fig. 4(b), the lifetime of the FER state is estimated to be 1.26–2.19 fs with $\hbar/\Delta E$. On the other hand, the round-trip time is 1.73–2.69 fs for the same F_{FER} range. The lifetime and the round-trip time have the same order of magnitude.

The transmission and light emission are two independent pathways for WFD; a constant D indicates that Γ_t and Γ_l are constant. Because Γ_l is irrelevant to the surface orientation and Γ_t is 0 for Ag(100), D on Ag(100) should be constant but smaller than that on Ag(111). Although Fig. 4(a) indicates that D on Ag(100) is indeed smaller, the drastic fluctuation of $1/\Delta E$ reflects that Γ_l is highly unstable. Figure 4(c) displays two (thin and thick) spectra on Ag(100), in which while the FER energies of orders from 1 to 3 are nearly identical, for the order >3 , the positive energy shift obviously appears and increases with order, as shown in the inset. Figures 4(d) and 4(e) display that ΔE of FER 1 can vary by up to a factor of four even under the same F_{FER} , which is reminiscent of quantum trapping [29].

Quantum trapping manifesting in ΔE originates from the following mechanisms: (1) Through the exchange interaction, two resonant electrons with opposite spins are successively

emitted from the tip to occupy the FER quantized state per unit time. (2) One electron emits light first to become a relaxed electron momentarily trapped in a potential well beneath the STM tip because of quantum trapping. (3) Both the relaxed electron and resonant electron have the same spin. Because of the Pauli exclusion principle, the resonant electron cannot emit light while the relaxed electron remains trapped in the well. Thus, the lifetime of the resonant electron is controlled by the relaxed electron. Due to these mechanisms, the WFD of relaxed electrons takes over that of resonant electrons emitting light subsequently.

Because a metallic surface cannot be penetrated by an electric field, the potential on the Ag surface remains constant [Fig. 5(a)] even when the tip structure consists of a base with a radius of tens of nanometers and a protrusion with atomic-scale sharpness (marked by an arrow). The open angle of the protrusion defines the sharpness of an STM tip. We suggest that a potential well can still be formed if the surface dipole layer (SDL) is involved. The SDL originates from the electrons that spill into the vacuum region to form a negatively charged layer [Fig. 5(b)], and thereby, a positive charge layer is created near the surface [41]. According to electrostatics, the field on a metal surface is constant if the base is flat [42]. Let us assume that the constant field is sufficiently strong to block

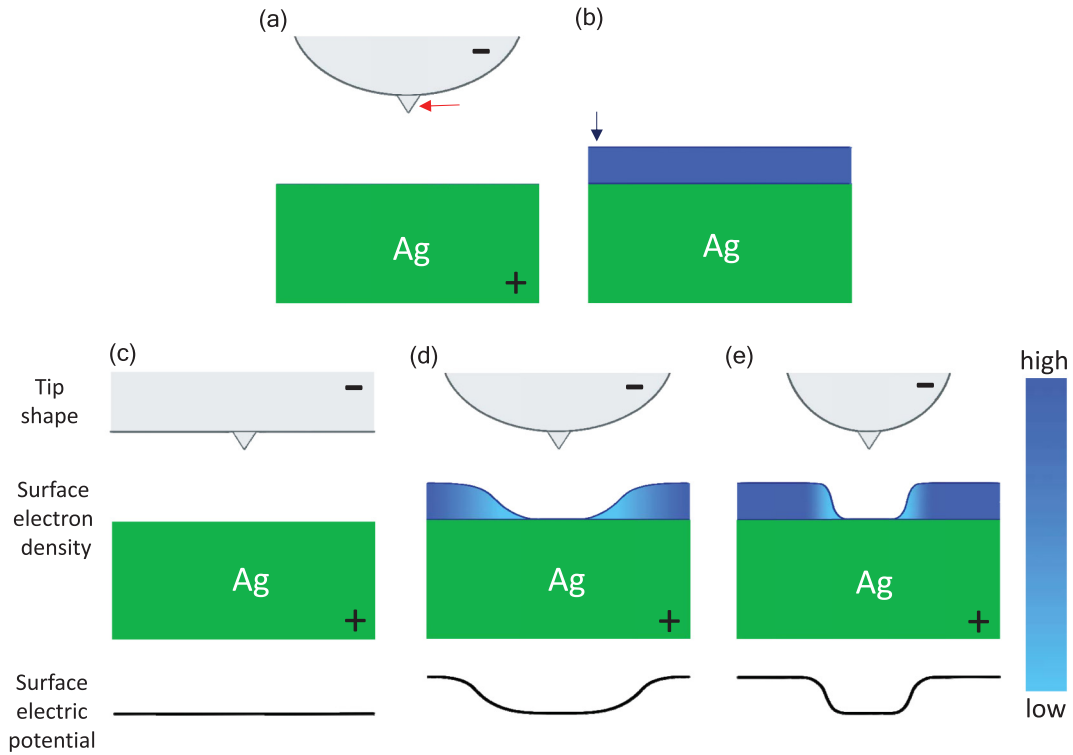


FIG. 5. Step-by-step illustrations of formation of a potential well on the Ag surface beneath a scanning tunneling microscopy (STM) tip (see text).

electrons to spill out [Fig. 5(c)]. When the base has curvature, beneath the protrusion, there still exists a local region where the field on the surface remains constant. The field outside this region decreases with the distance from the region center. Consequently, the electron density (scale bar) and its range outside the constant-field region gradually increase from zero to the values in the absence of a field, because of which a potential well for relaxed electrons exists on the surface, as depicted in Fig. 5(d). Figure 5(e) displays that the well size should be smaller than that in Fig. 5(d) when the same protrusion is on a base with a smaller radius.

Figure 4(c) implies that, for these two spectra, the protrusions had the same sharpness, but the base radius for the thin spectrum was larger than that for the thick spectrum because, for order >3 , data points in the FER energy of the former vs $(n-\frac{1}{4})^{2/3}$ plot follows the linear fit, whereas those in the latter one do not [Fig. 4(f)]. A larger base can contribute a stronger electric field to cause a higher FER energy. Therefore, Fig. 4(d) [4(e)] corresponds to Fig. 5(d) [5(e)]. Because of the intervention of the quantum trapping sensitive to the tip structure, ΔE on Ag(100) inevitably fluctuated. The narrow FER in Fig. 4(d) is related to resonance trapping [29]. The quantum trapping effect on Ag(100) proves the existence of the SDL.

Because of the energy gap, light emission is the only channel through which paired resonant electrons can leave FER, enabling the coexistence of a relaxed electron and a resonant electron. If no energy gap exists, the probability that a pair of resonant electrons both emit light is reduced to $(\frac{\Gamma_i}{\Gamma_i+\Gamma_j})^2$ due to transmission. Moreover, relaxed electrons engaging in reso-

nance trapping are unable to considerably prolong the lifetime of resonant electrons through the Pauli exclusion principle because of the aforementioned transmission. Due to these two factors, the signal of resonance trapping on Ag(111) is weak, which results in slight fluctuation [Fig. 4(b)].

Strong fluctuation can also be observed on Cu(100) because of the energy gap [43] (see Supplemental Material [37]). Moreover, because Cu has an electron density larger than Ag [44], SDL on Cu(100) is greater than that on Ag(100). Therefore, based on Fig. 5, it can be expected that, under the same F_{FER} and base radius, D ($\Delta E/F_{\text{FER}}^{2/3}$) on Cu(100) is different from that on Ag(100) because the well size on Cu(100) is larger. We measured ΔE of FER 1 on Cu(100) and Ag(100) under the same base at different currents (see Supplemental Material [37]) to investigate this issue. Figure 4(g) displays D vs F_{FER} plots for Ag and Cu, revealing different features that, within the same F_{FER} range (marked by dashed lines), the plot on Cu is a curve with a local maximum, whereas that on Ag is nearly constant. Therefore, Cu(100) and Ag(100) have dissimilar SDLs, as expected.

IV. CONCLUSIONS

In summary, we demonstrate that WFD differs noticeably on Ag(111) and Ag(100) surfaces because of their dissimilar band structures. Because Ag(111) has no energy gap, two resonant electrons emitted from the tip through the exchange interaction can leave FER through transmission. Consequently, electrons leaving FER through light emission are fewer than those on Ag(100), which results in an almost

stable dissipation rate involving weak quantum trapping signal. By contrast, WFD on Ag(100) is influenced by a strong resonance trapping effect that is sensitive to the structure of the STM tip and the SDL, causing considerable fluctuation in the dissipation rate. Through FER linewidth, we also demonstrate that the SDLs of Cu(100) and Ag(100) are dissimilar, which cannot be investigated using STM under the normal tunneling condition because the electric field in the STM junction may alter the electron layer.

ACKNOWLEDGMENTS

The authors are grateful for the support provided by the Ministry of Science and Technology (Grants No. MOST 109-2112-M-001-049 and No. MOST 109-2112-M-007-034-MY3) and Academia Sinica (Grant No. AS-iMATE-109-15), Taiwan. H.-T.J. also thanks the CQT-NTHU-MOE, NCHC, and CINC-NTU, Taiwan, for technical support.

-
- [1] K. H. Gundlach, *Solid State Electron.* **9**, 949 (1966).
- [2] G. Binnig, K. H. Frank, H. Fuchs, N. Garcia, B. Reihl, H. Rohrer, F. Salvan, and A. R. Williams, *Phys. Rev. Lett.* **55**, 991 (1985).
- [3] R. S. Becker, J. A. Golovchenko, and B. S. Swartzentruber, *Phys. Rev. Lett.* **55**, 987 (1985).
- [4] K. Bobrov, A. J. Mayne, and G. Dujardin, *Nature (London)* **413**, 616 (2001).
- [5] S. Liu, M. Wolf, and T. Kumagai, *Phys. Rev. Lett.* **121**, 226802 (2018).
- [6] P. S. N. Barimar, B. Naydenov, J. Li, and J. J. Boland, *Appl. Phys. Lett.* **110**, 263111 (2017).
- [7] J. Coombs, J. Gimzewski, B. Reihl, J. Sass, and R. Schlittler, *J. Microsc.* **152**, 325 (1988).
- [8] J. Martínez-Blanco and S. Fölsch, *J. Phys.: Condens. Matter* **27**, 255008 (2015).
- [9] C. C. Leon, A. Rosławska¹, A. Grewal, O. Gunnarsson, K. Kuhnke, and K. Kern, *Sci. Adv.* **5**, eaav4986 (2019).
- [10] J. I. Pascual, C. Corriol, G. Ceballos, I. Aldazabal, H. P. Rust, K. Horn, J. M. Pitarke, P. M. Echenique, and A. Arnau, *Phys. Rev. B* **75**, 165326 (2007).
- [11] P. Wahl, M. A. Schneider, L. Diekhoner, R. Vogelgesang, and K. Kern, *Phys. Rev. Lett.* **91**, 106802 (2003).
- [12] K. Schouteden and C. Van Haesendonck, *Phys. Rev. Lett.* **103**, 266805 (2009).
- [13] S. Stepanow, A. Mugarza, G. Ceballos, P. Gambardella, I. Aldazabal, A. G. Borisov, and A. Arnau, *Phys. Rev. B* **83**, 115101 (2011).
- [14] F. Craes, S. Runte, J. Klinkhammer, M. Kralj, T. Michely, and C. Busse, *Phys. Rev. Lett.* **111**, 056804 (2013).
- [15] C. L. Lin, S. M. Lu, W. B. Su, H. T. Shih, B. F. Wu, Y. D. Yao, C. S. Chang, and T. T. Tsong, *Phys. Rev. Lett.* **99**, 216103 (2007).
- [16] H. S. Huang, W. Y. Chan, W. B. Su, G. Hoffmann, and C. S. Chang, *J. Appl. Phys.* **114**, 214308 (2013).
- [17] F. Schulz, R. Drost, S. K. Hämäläinen, T. Demonchaux, A. P. Seitsonen, and P. Liljeroth, *Phys. Rev. B* **89**, 235429 (2014).
- [18] Z. Li, H. Y. Chen, K. Schouteden, E. Janssens, C. V. Haesendonck, P. Lievens, and G. Pacchioni, *Nanoscale* **7**, 2366 (2015).
- [19] K. Schouteden, B. Amin-Ahmadi, Z. Li, D. Muzychenko, D. Schryvers, and C. V. Haesendonck, *Nat. Commun.* **7**, 14001 (2016).
- [20] C. Gutiérrez, L. Brown, C. J. Kim, J. Park, and A. N. Pasupathy, *Nat. Phys.* **12**, 1069 (2016).
- [21] Q. Zhang, J. Yu, P. Ebert, C. Zhang, C. R. Pan, M. Yin. Chou, C. K. Shih, C. Zeng, and S. Yuan, *ACS Nano* **12**, 9355 (2018).
- [22] B. Borca, C. Castenmiller, M. Tsvetanova, K. Soththewes, A. N. Rudenko, and H. J. W. Zandvliet, *2D Mater.* **7**, 035021 (2020).
- [23] K. Sagisaka and D. Fujita, *Phys. Rev. B* **77**, 205301 (2008).
- [24] E. D. L. Rienks, N. Nilius, H. P. Rust, and H. J. Freund, *Phys. Rev. B* **71**, 241404(R) (2005).
- [25] W. B. Su, S. M. Lu, C. L. Lin, H. T. Shih, C. L. Jiang, C. S. Chang, and T. T. Tsong, *Phys. Rev. B* **75**, 195406 (2007).
- [26] W. Y. Chan, S. M. Lu, W. B. Su, C. C. Liao, G. Hoffmann, T. Ru. Tsai, and C. S. Chang, *Nanotechnol.* **28**, 095706 (2017).
- [27] S. M. Lu, W. Y. Chan, W. B. Su, W. W. Pai, H. Lin. Liu, and C. S. Chang, *New J. Phys.* **20**, 043014 (2018).
- [28] W. B. Su, C. L. Lin, Chan, W. Y. Chan, S. M. Lu, and C. S. Chang, *Nanotechnol.* **27**, 175705 (2016).
- [29] W. B. Su, S. M. Lu, H. T. Jeng, W. Y. Chan, H. H. Chang, W. W. Pai, H. L. Liu, and C. S. Chang, *Nanoscale Adv.* **2**, 5848 (2020).
- [30] S. Schuppler, N. Fischer, Th. Fauster, and W. Steinmann, *Phys. Rev. B* **46**, 13539 (1992).
- [31] L. E. Ballkntine, *Rev. Mod. Phys.* **42**, 358 (1970).
- [32] M. Schlosshauer, *Rev. Mod. Phys.* **76**, 1267 (2004).
- [33] A. Tonomura, J. Endo, T. Matsuda, and T. Kawasaki, *Am. J. Phys.* **57**, 117 (1989).
- [34] G. Kresse and D. Joubert, *Phys. Rev. B* **59**, 1758 (1999).
- [35] G. Kresse and J. Furthmuller, *Phys. Rev. B* **54**, 11169 (1996).
- [36] J. V. Barth, H. Brune, G. Ertl, and R. J. Behm, *Phys. Rev. B* **42**, 9307 (1990).
- [37] See Supplemental Material at <http://link.aps.org/supplemental/10.1103/PhysRevB.105.195411> for additional calculation details for Au(111), spectra due to spontaneous changes of tip sharpness acquired on Ag(100) and Cu(100), and spectra under different currents acquired on Ag(111), Ag(100), and Cu(100).
- [38] P. M. Echenique, J. M. Pitarke, E. V. Chulkov, and A. Rubio, *Chem. Phys.* **251**, 1 (2000).
- [39] W. Berthold, U. Höfer, P. Feulner, E. V. Chulkov, V. M. Silkin, and P. M. Echenique, *Phys. Rev. Lett.* **88**, 056805 (2002).
- [40] J. J. Sakurai, *Modern Quantum Mechanics*, 1st ed. (Benjamin-Cummings, New York, 1985), p. 104.
- [41] N. D. Lang and W. Kohn, *Phys. Rev. B* **1**, 4555 (1970).
- [42] M. H. Nayfeh and M. K. Brussel, *Electricity and Magnetism* (John Wiley & Sons, New York, 1985), p. 49.
- [43] A. Goldmann, V. Dose, and G. Borstel, *Phys. Rev. B* **32**, 1971 (1985).
- [44] N. W. Ashcroft and N. D. Mermin, *Solid State Physics* (Saunders College, Philadelphia, 1976), p. 5.